Coupling between ferromagnetic and ferroelastic transitions and ordering in Heusler alloys produces new multifunctionality

Oleg Heczko,* Hanuš Seiner, and Sebastian Fähler

The ability of Heusler alloys to accommodate broad variations of composition, doping, and ordering provides multiple options for tailoring their ferromagnetic and ferroelastic properties. Moreover, existing coupling between these ferroic properties ranging from coupled ferroic transitions to a coupling of their ferromagnetic and ferroelastic microstructure allows for manifold multifunctionalities. Here, we focus on ferromagnetic, metamagnetic and reentrant shape-memory alloys explaining the principles and sketch effects' rich susceptibility to temperature, magnetic field, and stress. We illustrate how these can provide a path to a multitude of emerging applications for actuation, sensing, and energy use. As an outlook, we discuss time dependency, fatigue, and finite size effects, which are not yet fully explored.

Introduction

In the 1990s, the discovery of reversible diffusionless phase transitions in the Ni–Mn–Ga alloy[1] (and shortly after also in several similar alloys)[2,3] brought a new impetus to the field of Heusler compounds, which finally led to emergence of a completely new class of materials: the ferromagnetic shape-memory alloys (FSMAs). The chemical and magnetic orderings known for the Heusler compounds for decades[4] couple with the ferroelastic ordering arising from phase transformation. This coupling gives rise to novel functionalities. Despite being all based on a limited number of elements, and despite all exhibiting the same cubic $L2_1$ Heusler structure in the high-temperature parent phase, the FSMAs show an astonishing variety of magnetomechanic, magnetocaloric, or mechanocaloric behaviors. All these phenomena in FSMAs are quite sensitive to even very small changes in the composition or heat treatment, which allows fine-tuning of the performance of the given material for specific applications.

The transformation occurring in FSMAs is so-called martensitic transformation. This means first-order displacive phase transition, where the lattice of the low-temperature phase (called martensite) differs from the lattice of the high-temperature phase (called austenite) by spontaneous symmetry-breaking strains. Martensitic transformation is well known in steels, which appears during quenching. The martensite in steel, however, can be reverted into austenite only by a diffusive annealing process contrary to FSMAs and shape-memory alloys in general, where the transformation is reversible and athermal (i.e., independent on the temperature change rate), and except for a small temperature hysteresis it is fully reversible.

The spontaneous strains in the low-temperature phase induce ferroelastic ordering forming homogeneous regions of the lattice with the same crystal orientation. These are called variants of martensite, and the variants tend to arrange spatially by twinning into ordered microstructures, so-called martensitic laminates.[5]

Without coupling between ferroelasticity and ferromagnetism the functional pathways are limited just to the conventional shape-memory effect and superelasticity. The former is well known from nonmagnetic shape-memory alloys such as NiTi or Cu–Al–Ni and can be described as follows: Cooling below the martensitic transformation temperature turns austenite into a mixture of martensitic variants connected by sharp

Oleg Heczko, Faculty of Mathematics and Physics, Charles University, Prague, Czech Republic; FZU–Institute of Physics, The Czech Academy of Sciences, Prague, Czech Republic; heczko@fzu.cz
Hanuš Seiner, Institute of Thermomechanics, The Czech Academy of Sciences, Prague, Czech Republic
Sebastian Fähler, Institute of Ion Beam Physics and Materials Research, Helmholtz-Zentrum Dresden-Rossendorf, Dresden, Germany
*Corresponding author
doi:10.1557/s43577-022-00354-x

interfaces called twin boundaries. In the simplest case, a twin boundary can be considered as a mirror plane between two variants with different crystal orientations (e.g., a (101) plane) separating variants with spontaneous strain in the [100] and [001] directions, as sketched in **Figure 1** in two dimensions. Under external mechanical loading, martensite can accommodate inelastic strains through reorientation, that is, moving the twin boundaries such that the variants oriented favorably to the loading grow while the others shrink. At the macroscale it results in a change of the sample shape, and this change is seemingly plastic, which means it remains stable after the loading is removed. It can be, however, erased by heating the material up above the martensite → austenite transition temperature so that the original shape of the material is recovered. Accordingly, this effect is called shape-memory effect (Figure 1a). Related to this is the superelasticity pathway (Figure 1b), where the austenite above the transition temperature is turned into martensite by application of stress. Due to the stress, the martensite is already oriented, which results in a large macroscopic strain of the sample. This strain disappears when the loading is removed because the martensite is unstable at the given temperature. This first-order martensitic transformation is associated with a latent heat and thus the sample temperature changes when it is strained adiabatically. This enables the so-called elastocaloric effect, which promises a path for environmentally friendly refrigeration.[6]

Although both these phenomena are already fascinating and predetermine the shape-memory alloys for a broad range of smart applications, the behavior, as it will be discussed in this article, becomes much richer due to the presence of the second ordering, ferromagnetism. Figure 1 outlines known-to-date functionality pathways of FSMA materials.

The simultaneously appearing and mutually coupled ferromagnetic and ferroelastic orderings provide for a broad variety of unique behaviors typical for multiferroics. The coupling can take different forms: it may enable the martensitic transitions and the martensitic microstructures to be controlled by the external magnetic field, which gives rise to the metamagnetic effects[7] (Figure 1e–f) or magnetically induced reorientation (MIR) (Figure 1c) and stray field induced actuation.[8] Moreover, the competition between ferromagnetic and ferroelastic orderings facilitates several counterintuitive phenomena, such as the inverse magnetocaloric effect[9] or the appearance of the reentrant austenite phase.[10] Depending on the particular alloy and on the temperature range where the loadings are applied, external mechanical or magnetic fields can initiate just reorientation in the martensite phase (MIR), as explained in the next section and discussed in connection with twinning hierarchy and enhanced magnetic hysteresis in the following section. Alternatively, the field can initiate either the forward or reverse martensitic transitions resulting in magnetically induced austenite (MIA) and martensite (MIM), as described in the section "Metamagnetic transitions." Reentrant behavior arising from excess magnetic entropy is sketched in the following section. The final section brings the outlook of less explored features of these effects.

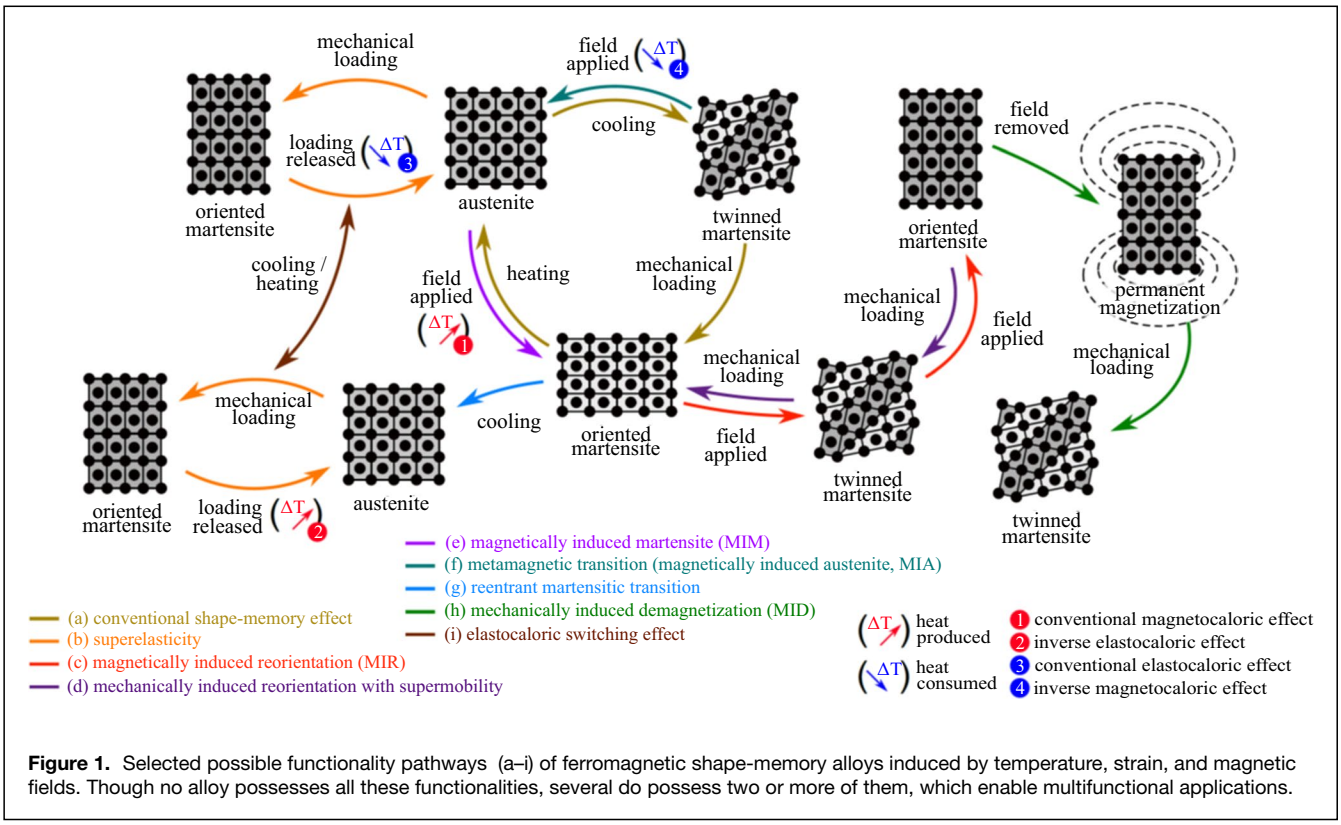

Figure 1. Selected possible functionality pathways (a–i) of ferromagnetic shape-memory alloys induced by temperature, strain, and magnetic fields. Though no alloy possesses all these functionalities, several do possess two or more of them, which enable multifunctional applications.

Ferromagnetic shape-memory phenomena

When the martensite phase is in the ferromagnetic state, which means below the Curie point, the ferromagnetic ordering appears and a microstructure of magnetic domains arises. The easy magnetization axis of the martensitic lattice is typically aligned with the shortest lattice parameter, and, consequently, the magnetic domains arrange so that the magnetization vector lies almost everywhere along the shortest axis. However, the magnetization is a *vector*, and a martensitic variant has an *orientation*, and thus, magnetic domains with two antiparallel orientations occur within each variant. When an external field is applied, the magnetization rotates toward the direction of the field. In the particular case of FSMAs, provided that the lattice is very pliable and the coupling of magnetization to the lattice is strong, the lattice can be dragged by the rotating magnetization, and the reorientation of martensite ensues (Figure 1c). In this case, a virgin magnetization curve exhibits a pronounced hysteresis in the first quadrant[11,12] signifying the magnetically induced reorientation (MIR).[12] The reorientation results in large magnetic field induced strains (MFIS) as shown in **Figure 2**a.

The deformation from MIR is pseudoplastic, which means it is stable after the field is removed and can be reversed by an external force or field applied in another direction. Since the spontaneous distortion of the lattice is usually large, full reorientation can result in a large macroscopic effect: the maximum of experimentally observed MFIS stands now at about 12%[13]—two orders of magnitude larger than the so-called giant magnetostriction. The theoretical maximum considering the existing phases can reach up to 20%.[14] Importantly, due to the axial symmetry of magnetic field and lattice distortion, the MIR is always associated with rotations of the easy axis by 90°.

The energy balance of the MIR effect can be captured by a simple model.[11,12,15] The reorientation occurs only if the difference of magnetic (volume) energies between differently oriented twin variants is larger than the volume work needed for the reorientation, where the latter can be expressed as $\sigma_{tw}\varepsilon_0$. Here, σ_{tw} is the twinning stress and ε_0 is the lattice deformation.

As shown graphically in Figure 2a, the maximum work output of the MIR effect is limited by magnetocrystalline anisotropy K_u. The higher anisotropy, the more is the magnetization resistant against rotating out of the magnetically easy axis, and thus, the external field translates into a stronger torque or driving force for reorientation. Hence, finding the way how to increase K_u is highly desirable but rather unknown. The anisotropy is not particularly strong in the martensite phases of Heusler alloys ($K_u \approx 10^5$ J/m^3 for Ni–Mn–Ga), and, consequently, material must exhibit a very small twinning stress to enable MIR, even if no external load is applied.

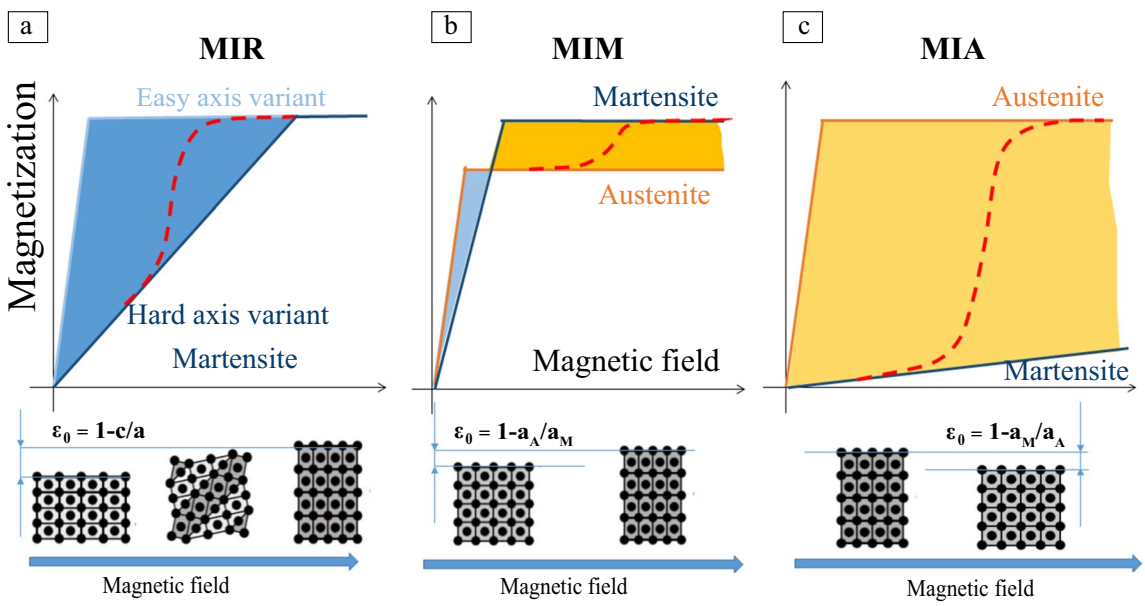

Figure 2. Magnetic energy available for the magnetically induced reorientation (MIR) and magnetically induced transformations (filled area between magnetization curves) and magnetization changes related to the effects (red broken line). The maximum strain is obtained from lattice reorientation (the difference between lattice constants of tetragonal martensite) or phase transformation (the difference between cubic and tetragonal lattice constants) as sketched. For MIR (a), the energy is given by the difference between the magnetization curves for two differently oriented martensite variants and thus ultimately by magnetocrystalline anisotropy. Once the magnetic saturation is reached, the field increase does not increase the energy. This can be contrasted with (b) magnetically induced martensite (MIM) and (c) magnetically induced austenite (MIA) pathways, in which the magnetic energy can increase indefinitely with the increasing external field, depending on the magnetization difference between the phases.

The main representatives of the alloys with MIR are Ni–Mn–Ga alloys close to the Heusler stoichiometry Ni_2MnGa,[14] and some derivatives alloyed by small amounts (up to 5%) of Fe, Co, and Cu.[16,17] The properties of these alloys are discussed in more detail in the next section. Several other Heusler alloys may also possess the required combination of strong magnetocrystalline anisotropy and high mobility of twin boundaries, as summarized in Reference 18, but these systems have not yet been sufficiently explored by experiments. The largest MIR effect is observed in single crystals, as the grain boundaries put constraints on the twin boundary motion. These constraints can be partly removed using low-dimensional materials as thin wires and whiskers[19] or foams.[20] Such material can substitute the complex mechanical arrangement fulfilling the saying—the materials are the machine.[21]

Using a similar graphical representation of the energy balance as for MIR, also the effects of magnetically induced martensite (MIM) or magnetically induced austenite (MIA) can be captured, as shown in Figure 2b–c with pathways in Figure 1e–f. In both effects the magnetic field induces a phase transition, and thus the magnetic field replaces a temperature change in the vicinity of the transformation temperature. The MIM effect appears if the saturation magnetization of martensite is higher than that of austenite, which is the typical case for Ni–Mn–Ga Heusler alloys. Consequently, applying a magnetic field can initiate the transition from austenite to martensite. This relationship is reversed in alloys with low magnetic martensite and highly ferromagnetic austenite. In these materials, the magnetic field initiates the reverse transition to austenite. Such materials, a typical example being Ni–Co–Mn–In, exhibit the so-called metamagnetic behavior, which is discussed later.

Hierarchical twinning and supermobility in Ni–Mn–Ga

The compounds from the Ni–Mn–Ga Heusler family are certainly the most extensively studied FSMAs and also those most promising as candidates for magnetomechanical applications. The martensite phase in these alloys can be either tetragonal non-modulated (NM), or monoclinic modulated phases. The low symmetry of the martensite lattice (i.e., the monoclinic symmetry) has an important consequence for the morphology of the martensitic microstructures appearing in these alloys. The monoclinic martensite can form several types of twins. The twinning planes of different twinning types have different interface energies, and therefore tend to appear at different length scales, which results in higher-order laminations[22,23] and often even in a complex ferroelastic variants hierarchy,[24] such as the one shown in **Figure 3**.

Although the complexity of the twinning can be stunning, only the twin boundaries separating ferroelastic variants with different orientations of the magnetization can be manipulated by the magnetic field. These are the so-called *a*/*c* twins at the mesoscale, where the *c*-axis is the shortest magnetically easy axis with which the magnetization tends to be aligned, while *a* and *b* crystal axes are magnetically hard axes. In Ni–Mn–Ga single crystal, the *a*/*c* twin interface acts as a two-dimensional macroscopic object, sweeping and rearranging the whole volume of the sample[25] during MIR. Each of the other types of

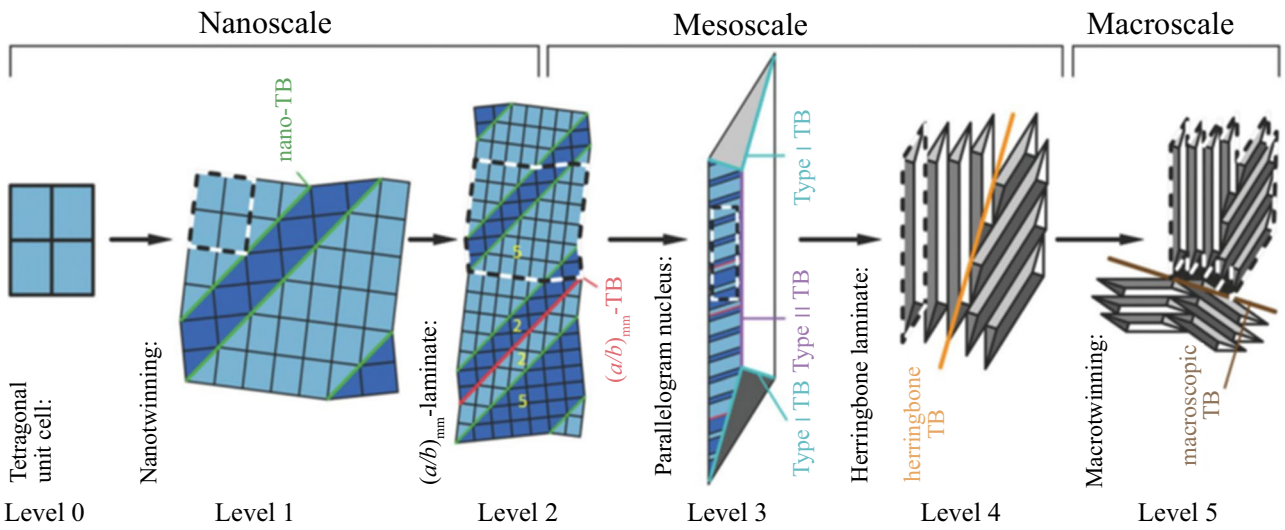

Figure 3. A deep hierarchy of twins within twins, as exemplarily observed in epitaxial Ni–Mn–Ga films in the 14M modulated martensite (mm) phase.[24] This microstructure forms due to a combination of low-symmetry class of the martensite unit cell and compatibility constraints put on the film from a rigid substrate. It spans several length scales and each building block (hatched area) is required to build the next level. It starts from the tetragonal unit cell (level 0) and forms different types of twin boundaries (TB) due to the need to form an almost (level 1) and exactly (level 2) compatible phase boundary between austenite and martensite, the need to nucleate martensite within austenite (level 3), to transform the complete volume (level 4), and the different orientations possible (level 5).

TB, as sketched in Figure 3, responds to a particular constraint of the martensitic transformation. Although the role of the other types of twinning is not entirely clear, it can be assumed that TB at the nanoscale are an integral part of mesoscopic *a/c* twin boundaries securing the extreme mobility,[26] while TB at the macroscale are hindering their motion. In a monoclinic lattice, there are two types of *a/c* twin boundaries, Type I and Type II using the classification of twins from Reference 5. In Ni–Mn–Ga modulated martensite, both types are extremely mobile or, in other words, a very low mechanical stress is sufficient to set them into motion (Figure 1d). In the 10M modulated martensite the Type I twin boundary can be moved under the stress of about 1 MPa, while the Type II under the stress even below 0.05 MPa, if there are no obstacles for their motion.[25] Such small stress corresponds to a small magnetic field about 20 mT or 16 kA/m^2 depending on sample geometry. There can also exist mixed twin boundaries, composed of segments of Type I and Type II, for which the stress is between these two limits.[27]

The twinning stress for the Type II twin boundary is by two orders of magnitude lower than in conventional SMAs such as Ni–Ti, or in NM martensite of Ni–Mn–Ga. This extreme softness is exceptional and has not been observed in any other material yet. This softness is best illustrated that you can deform a sample with your fingertips like rubber—in contrast to martensitic steel, which can be extremely hard. But the miracle does not end here. Whereas the twinning stress for the Type I twin boundary is strongly temperature-dependent and rapidly increases with cooling, the twinning stress for Type II exhibits just a very weak temperature dependence, which enables extending the MIR effect to the lowest temperatures.[28,29] The experimentally demonstrated high mobility of Type II twins at 1.7 K indicates that the motion of these interfaces does not require thermal activation, or, at least, that there are extremely small barriers the thermal activation needs to overcome. Hence, we can really talk about the supermobility of the twin boundary.

What causes the supermobility and why it occurs particularly in the Ni–Mn–Ga compound has not been resolved yet.[30,31] Most probably, it is closely related to the existence and properties of the modulations[32–35] that are metastable with respect to the NM structure and can also transform one into another via the intermartensitic transitions.[11,36] Nevertheless, the existence of the supermobile behavior itself opens brand new possibilities for technological applications of Ni–Mn–Ga, ranging from remotely controlled micropumps for medication[37] to hybrid composite structures with field-controlled damping properties[38] and due to insignificant temperature dependence also in space. Several prototypes and suggested applications are shown in **Figure 4**, illustrating the pathway of a large stroke actuator (a) and combined pathway used in a circuit breaker (b). This benefits from the combination of two pathways: high overcurrent induces a magnetic field, which breaks the circuit by the MIR effect fast, and to shut down at low overcurrent after quite some time, Joule heating is used to induce the shape-memory effect.

One of the current directions in the application-oriented research is the attempt to couple the supermobility with the magnetic hysteresis in Ni–Mn–Ga single crystals. In the currently used alloys, the magnetic hysteresis or coercivity force is negligible, despite relatively large magnetocrystalline anisotropy. As a result, the magnetic domain structure is wiped out in much weaker fields than those needed to trigger the reorientation, and, therefore, the magnetic domain structure has no significant effect on MIR.[39,40] However, one can consider the coercivity as an additional free parameter that can modify the multiferroic behavior. Recently, we showed that if the coercivity is enhanced, new functionality can arise.[41] Such material can exhibit the mechanically induced demagnetization (MID, Figure 1h), and can be used for energy harvesting in a very simple arrangement.[42,43] The coercivity can be enhanced mainly by defects in the lattice, and by the increased concentration of antiphase boundaries in particular.[44,45] The antiphase boundaries, although responsible for strong magnetoelastic softening in austenite[46] and huge non-ergodic magnetoelastic damping in premartensite,[47] do not significantly affect the motion of Type I and Type II twins in martensite, and are, therefore, an optimal tool for controlling the magnetic hysteresis without compromising the supermobility.

Metamagnetic transitions

The magnetically induced strains discussed in the previous section originate from the reorientation of martensitic variants below martensitic transformation. Another possibility for the shape change is to induce magnetically the austenite ↔ martensite transition itself resulting in the MIM/MIA effect (Figure 1e–f). In contrast to MIR, this phenomenon utilizes the difference of spontaneous magnetizations of austenite and martensite and can be induced only in the vicinity of transformation temperature. In a magnetic field, the phase exhibiting the higher magnetization is favored thermodynamically.

The MIM effect (Figure 2b) occurs also in Ni–Mn–Ga materials known for MIR. To obtain significant deformation in martensite additional mechanical prestress is required.[48–50] Thus, more attention is paid to the materials undergoing the so-called metamagnetic transitions from martensite to austenite. The main examples of such alloys are Ni–Mn–*X* (*X* = In, Sn, Sb)[51–54] and in particular Ni–Co–Mn–In,[7,55,56] which is nowadays understood as a prototypical metamagnetic shape-memory material exhibiting MIA.

These alloys exhibit nearly nonmagnetic martensite, being paramagnetic or antiferromagnetic, and strongly ferromagnetic austenite. As a result, the magnetic field can easily trigger the reverse transition to austenite resulting in magnetically induced shape recovery. The scheme of magnetic energy triggering the transformation is illustrated in Figure 2c. There are two important features of the metamagnetic transitions. The first is that the martensite → austenite transition allows for a much higher work output (higher magnetostress) than reorientation of martensite in MIR, as it results from the mechanical stiffness of austenite.[57] This predetermines metamagnetic

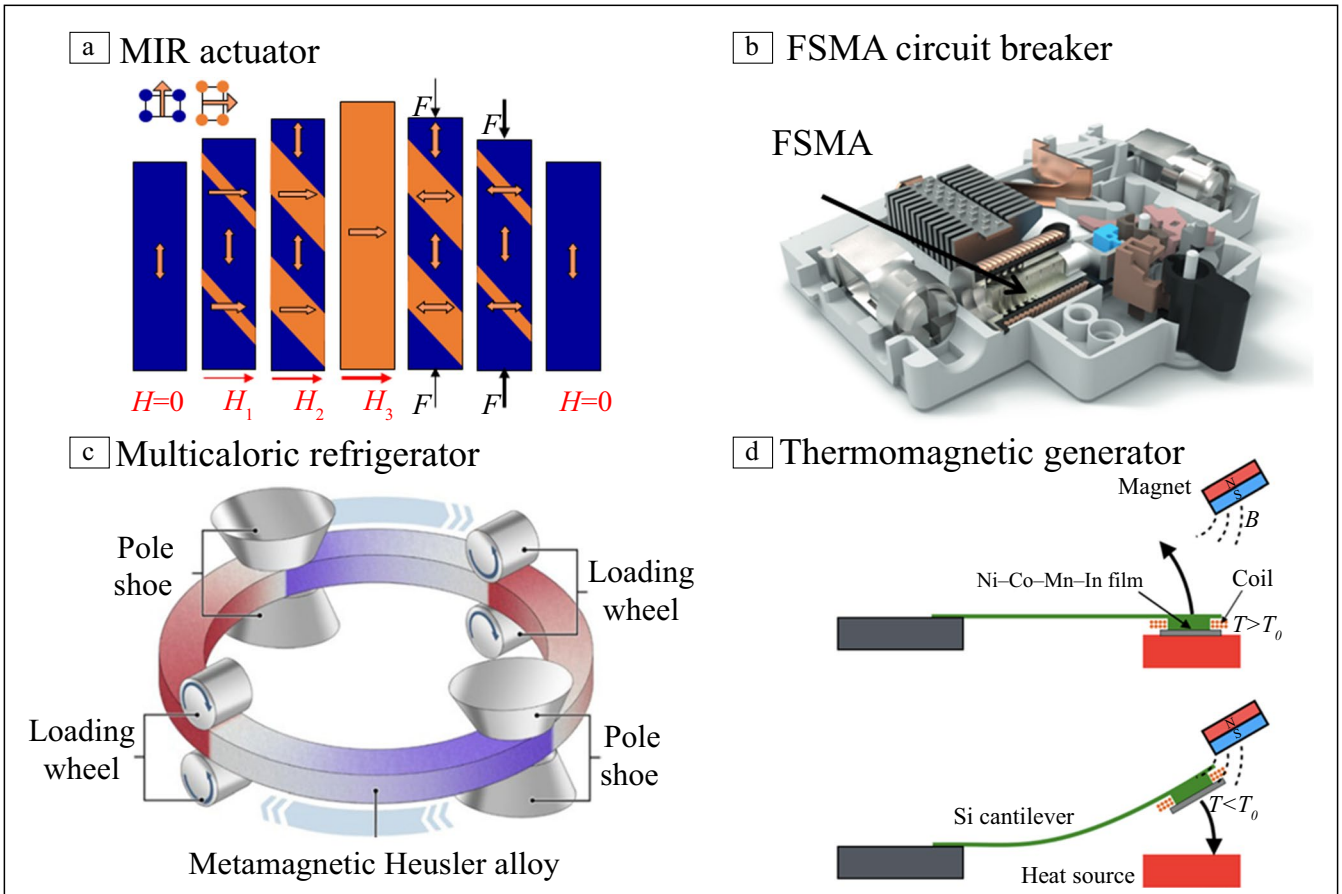

Figure 4. Some existing and suggested applications and devices of ferromagnetic and ferroelastic Heusler alloys. (a) Large stroke actuator utilizing a magnetically induced reorientation (MIR) by a magnetic field *H* and restoring force *F* by a spring. Adapted from Reference 72. (b) Ferromagnetic shape-memory alloy (FSMA) circuit breaker, which quickly cuts the power by MIR when the current (within the field coil) is too high or slowly by the shape-memory effect when heating by the current is too high. Reproduced with permission from Reference 73. (c) Multicaloric refrigerator combines the magnetocaloric effect created by the pole shoe and the elastocaloric effect created by the loading wheel in order to circumvent the transformation hysteresis. Adapted with permission from Reference 74. (d) Micro-thermomagnetic generator: microcantilever oscillates between heat source and magnet due to huge magnetization change in a narrow temperature span in the Ni–Co–Mn–In film. An induction coil converts mechanical oscillations to electric energy. Adapted with permission from Reference 75.

materials to be used for magnetic actuation under high external mechanical loads. Moreover, by tuning the mechanical prestress, the magnetically used transition can be made nearly nonhysteretic, which might be favorable in the applications.

The second important feature of metamagnetic transition is the inverse magnetocaloric effect.[58–61] The magnetic transition from a nonmagnetic state to a ferro-state typically leads to a temperature increase, but in metamagnetic shape-memory alloys this increase is compensated by the latent heat consumption due to the first-order transition. As a result, the alloy can reduce its temperature by several kelvins (6.2 K reported for the Ni–Co–Mn–In at 315 K in a 2 T field),[55] which makes the metamagnetic alloys perfect candidates for applications in magnetic refrigeration. To fully exploit this potential, there is a need to shift the metamagnetic transition temperature to the room temperature, and either to minimize the hysteresis by varying the chemical composition (see References 55, 62, and 63), or to design the cooling device (Figure 4c) such that the magnetic force acts against a mechanical prestress,[57] which suppresses the hysteresis.

Several prototypes of metamagnetic-cooling devices have already been designed,[9] many of them utilizing the facts that the inverse magnetocaloric effect can be achieved in relatively low fields and in low-dimensional materials (films, wires, ribbons). Additional attention is also paid to the reversibility of the transition, cyclic stability, and fatigue life of the magnetocaloric component, all of them being key prerequisites for real-life refrigeration applications[64] and energy harvesting.[65] Closely related are thermomagnetic energy harvesting devices, which utilize the reverse effect to convert low grade waste heat to electrical energy.[66] These require a huge magnetization change in a narrow temperature range, and for microsystems (Figure 4d) Heusler alloys are the material of choice.[67]

Other important phenomena observed in FSMAs with metamagnetic transitions are large magnetoresistance[68] and

the thermal transformation arrest (TTA) or kinetic-arrest effect.[69,70] The former is demonstrated as a sharp change in electric resistance once the alloy is put into the external magnetic field. It is sometimes even called giant magnetoresistance to point out that this effect is in strength comparable to the quantum–mechanical magnetoresistance observed in nanoscale layered heterostructures.[71] Here, the effect originates from the big difference between electrical resistance of austenite, and the (metamagnetic) martensite → austenite transition initiated by the magnetic field.

The TTA effect is viewed as an interruption of the forward transition when the metamagnetic alloy is cooled down in a strong magnetic field. At a certain temperature, called the kinetic-arrest temperature T_{KA}, the system becomes "frozen" in a dual-phase state, and the residual austenite does not transform into martensite during further cooling and does not disappear even close to absolute zero. The reason for this unusual behavior is in the entropy change ΔS associated with the transition. ΔS has two components with different signs, one from the magnetic transition and one from the structural transition, and these two components compensate each other at T_{KA}. Consequently, the driving force for the transition undercooled by ΔT, which is $G \approx \Delta T \Delta S$, vanishes to zero. Due to the magnetostructural hysteresis the reverse transition into austenite does not occur and the incomplete transition comes on hold. The TTA phenomenon is unavoidable in metamagnetic Heusler alloys, and is considered undesirable for caloric applications, as it brings non-ergodicity into the magnetothermal behavior. On the other hand, the vanishing entropy difference between austenite and martensite enables, through the Clausius–Clapeyron rule, widening significantly the temperature window in which the given alloy can be used for magnetomechanical actuation.[63]

Reentrant austenite behavior

A unique form of the metamagnetic transition appears in the recently discovered class of Heusler alloys where the martensitic transition temperature is high above the Curie point. In the paramagnetic state, the entropy change ΔS has only its structural component, and thus, the austenite undergoes the "conventional" forward transition to martensite upon cooling. However, as soon as the Curie point for austenite is reached, the magnetic contribution to ΔS may prevail, and initiate the reverse transition (Figure 1g), despite the material being well below the M_f temperature. In some sense, this behavior can be seen as an extreme case of the TTA effect at zero external field, utilizing the complete reversal of the sign of ΔS at T_{KA}. Here, instead of the external field, the driving force for the transition comes from the incipient exchange interaction between magnetic moments.

Upon cooling, such an alloy then undergoes an austenite (paramagnetic) → martensite (nonmagnetic) → austenite (ferromagnetic) transformation sequence, where the low-temperature variety of austenite is called the reentrant austenite phase and the transition is called the reentrant martensitic transition.[10] Upon heating, a reverse sequence can be observed, where the reentrant cubic phase transforms first to martensite, and the martensite then undergoes a conventional reverse transition at high temperatures. A prototypical example of an alloy with the reentrant transition is the Co–Cr–Ga–Si alloy (with 51–54 at.% of cobalt), where the sign-reversal of ΔS appears at approximately $T_{KA} = 350$ K.[10,76] More recently, a similar phenomenon was observed also in the Co–Cr–Al–Si alloy.[77,78] Both these alloys have the Heusler $L2_1$ structure in both the low-temperature and high-temperature cubic phases, and chemical compositions close to Co_2CrX, where X is a mixture of Ga and Si or Al and Si, usually approximately to the 1:1 ratio.

The simplest experimental demonstration of the reentrant transition is the low-temperature shape recovery process, where the pseudoplastic strain achieved by the reorientation of martensite is erased by the reentrant transition in the same way as it is erased at high temperatures by the conventional shape-memory effect. Possible applications of this phenomenon have not been fully explored yet, but there is an obvious technological advantage in obtaining the stiff → soft → stiff sequence of mechanical responses in a single heating or cooling run instead of in a thermal cycle.

Another remarkable consequence of the sign-reversal of ΔS is the nonlinear Clausius–Clapeyron relationship between the temperature (T) and the critical stress for triggering the forward martensitic transition (σ_M). This is observed in alloys with less than 50 at.% Co that stay fully in the cubic phase in the whole temperature range, but are superelastic (i.e., they can undergo large reversible strains due to stress-induced austenite → martensite transitions). In conventional shape-memory alloys the $d\sigma_M/dT$ slope is a constant, whereas here it is negative at temperatures below T_{KA} and positive above it. The transition between $d\sigma_M/dT < 0$ and $d\sigma_M/dT > 0$ is gradual, and there exists a quite broad temperature window (~50 K) where the critical stress is approximately constant.[76] Several possible applications are also envisaged for the Co–Cr–Al/Ga–Si alloys in terms of elastocalorics, as the stress-induced austenite → martensite transitions can switch from endothermic to exothermic by passing across the T_{KA}. This so-called elastocaloric switching effect[78] enables the same material to act as either heat source, or heatsink, depending on whether it operates at high or low temperatures (Figure 1i).

Outlook

The map of pathways in Figure 1 is necessarily incomplete as there are new Heusler alloys with FSMA properties currently discovered and studied, and novel functionalities can be expected to arise. However, each application requires a particular optimum composition, and therefore the search for better Heusler alloys benefits from their large miscibility with many elements. Indeed, optimum stoichiometry often deviates strongly from X_2YZ—and accordingly in this article, we talk on Heusler alloys and not on compounds as in the other articles in this issue.

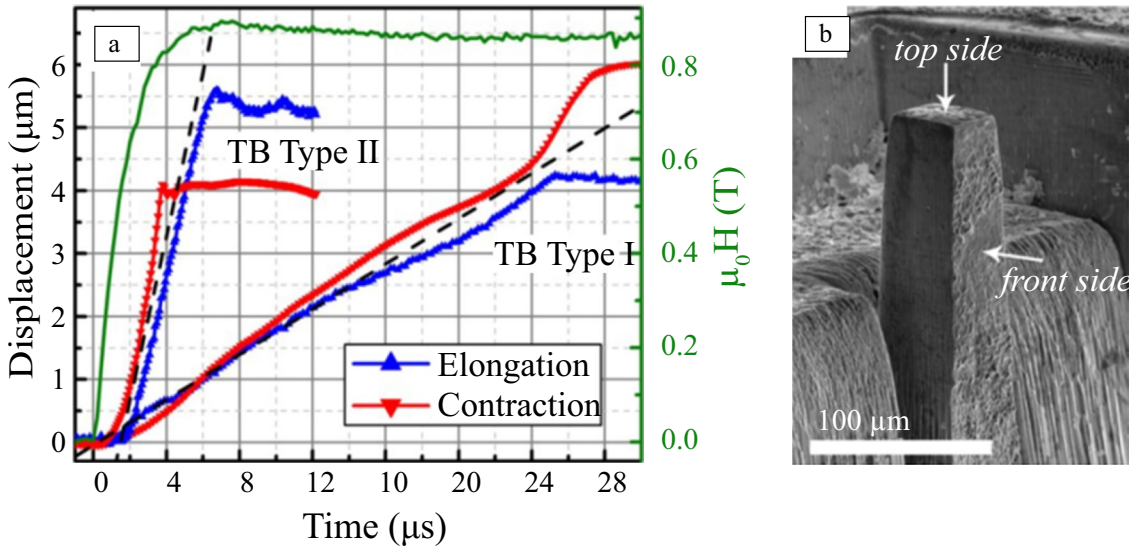

Figure 5. (a) Experimentally measured velocity of twin boundaries (TB) of Types I and II acting in a magnetically induced reorientation (MIR) pathway. Type II is much faster in response to the same field impulse. (b) A Ni–Mn–Ga micropillar exhibiting MIR. The large ratio between surface and volume and surface irregularities can block the motion of TB. Adapted from Reference 83 with permission.

With the large number of possible alloying elements and with the enormous sensitivity to the chemical composition, the Heusler FSMA systems obviously call for a high-throughput characterization, either using composition-spread experimental approaches,[79,80] or by means of theoretical computations (see Reference 30 for a review). However, both approaches are not fully satisfactory and have their limitations as thin films can strongly differ from bulk due to substrate constrains,[81] and theoretical approaches are challenged by the tiny energy differences of the competing structures. This leaves bulk experiments as benchmark.

Most of the described multifunction effects profits from a high working frequency as this increases the power linearly. Thus an emerging research topic is understanding and expanding the speed limits. While a ferroelastic transformation itself can be completed within 10 ns,[82] most applications based on the phase transformations are limited today to several Hz for bulk caloric devices or some 100 Hz for miniaturized thermomagnetic systems.[67] Although for all applications directly involving a phase transformation the frequency is limited by the heat exchange, this is not an issue for MIR. Experimentally, it was demonstrated that the actuation can in principle work at frequencies up to 100 kHz.[83] As shown in **Figure 5a**, the Type II boundary moves much faster compared to Type I when loaded by the same steep increase of the magnetic field, which illustrates the important role of the particular martensitic microstructure.

Importantly, it has also been shown that MIR generated by motion of few twin boundaries in a single crystal can withstand tens of millions of cycles in a rotating magnetic field[84] and even hundreds of millions under mechanical load.[85] For a finely twinned microstructure, in which the twin boundary moves for a short distance (e.g., in a peristaltic micropump),[37,86] the fatigue life can be even much longer. Although the fatigue issue can be solved for the pathways, where only the microstructure changes, it is still a challenge for all pathways involving phase transformations. The solution is to search for a highly compatible martensitic microstructure.[87]

While higher frequencies automatically require a longer cycle stability, these aspects are also connected with miniaturization as these smart materials allows keeping a system simple. However, not much is known on the impact of size effects on the different pathways. A key parameter appears to be the surface-to-volume ratio. For pathways, including a martensitic transformation, increasing the ratio accelerates heat exchange and thus frequency. On the other hand, it has an influence on the formation of twin boundaries[88] and also phase boundaries, which becomes more difficult and can ultimately block their motion. Although in conventional shape-memory alloys a sharp increase of the twinning stress with decreasing size has been reported,[89] Ni–Mn–Ga pillars with a size about 50 μm still exhibit MIR[83] (Figure 5b), and that actuation based on the transformation is possible even at the scale of 100 nm.[90] It seems that Feynman famous saying is valid here—there's still plenty of space at the bottom—to explore finite size effects.

Author contributions

All authors contributed equally.

Funding

Part of this work was supported by DFG through SPP FerroicCooling—FA453/12 (S.F.) and by the Czech Science Foundation, Grant No. 19-09882S (O.H.) and 21-06613S (H.S.) and by the Operational Program Research, Development and Education by MEYS CR within projects MATFUN –CZ.02.1.01/0.0/0.0/15-003/0000487.

Data availability

Not applicable.

Conflict of interest

There is no conflict of interest.

References

1. I.K. Zasimchuk, V.V. Kokorin, V.V. Martynov, A.V. Tkachenko, V.A. Chernenko, *Phys. Met. Metallogr.* **69**, 104 (1990)
2. F. Gejima, Y. Sutou, R. Kainuma, K. Ishida, *Metall. Mater. Trans. A* **30**, 2721 (1999)
3. K. Oikawa, T. Ota, F. Gejima, T. Ohmori, R. Kainuma, K. Ishida, *Mater. Trans.* **42**(11), 2472 (2001)
4. P.J. Webster, *Contemp. Phys.* **10**(6), 559 (1969)
5. K. Bhattacharya, *Microstructure of Martensite: Why It Forms and How It Gives Rise to the Shape-Memory Effect*, vol. 2 (Oxford University Press, Oxford, 2003)
6. D. Cong, W. Xiong, A. Planes, Y. Ren, L. Mañosa, P. Cao, Z. Nie, X. Sun, Z. Yang, X. Hong, Y. Wang, *Phys. Rev. Lett.* **122**, 255703 (2019)
7. R. Kainuma, Y. Imano, W. Ito, Y. Sutou, H. Morito, S. Okamoto, O. Kitakami, K. Oikawa, A. Fujita, T. Kanomata, K. Ishida, *Nature* **439**(7079), 957 (2006)
8. M. Thomas, O. Heczko, J. Buschbeck, Y.W. Lai, J. McCord, S. Kaufmann, L. Schultz, S. Fähler, *Adv. Mater.* **21**(36), 3708 (2009)
9. S. Fähler, V.K. Pecharsky, *MRS Bull.* **43**(4), 264 (2018)
10. X. Xu, M. Nagasako, M. Kataoka, R.Y. Umetsu, T. Omori, T. Kanomata, R. Kainuma, *Phys. Rev. B* **91**(10), 104434 (2015)
11. O. Heczko, A. Sozinov, K. Ullakko, *IEEE Trans. Magn.* **36**, 3266 (2000)
12. O. Heczko, N. Scheerbaum, O. Gutfleisch, *Nanoscale Magnetic Materials and Applications* (Springer, Boston, 2009), pp. 399–439
13. A. Sozinov, N. Lanska, A. Soroka, W. Zou, *Appl. Phys. Lett.* **102**, 021902 (2013)
14. N. Lanska, O. Söderberg, A. Sozinov, Y. Ge, K. Ullakko, V.K. Lindroos, *J. Appl. Phys.* **95**, 8074 (2004)
15. A.A. Likhachev, K. Ullakko, *EPJ Direct* **1**, 1 (2000)
16. M. Rameš, O. Heczko, A. Sozinov, K. Ullakko, L. Straka, *Scr. Mater.* **142**, 61 (2018)
17. A. Pérez-Checa, J.M. Porro, J. Feuchtwanger, P. Lázpita, T.C. Hansen, C. Mondelli, A. Sozinov, J.M. Barandiarán, K. Ullakko, V. Chernenko, *Acta Mater.* **196**, 549 (2020)
18. J. Pons, E. Cesari, C. Seguí, F. Masdeu, R. Santamarta, *Mater. Sci. Eng. A* **481**, 57 (2008)
19. N. Scheerbaum, O. Heczko, J. Liu, D. Hinz, L. Schultz, O. Gutfleisch, *New J. Phys.* **10**(7), 073002 (2008)
20. M. Chmielus, X.X. Zhang, C. Witherspoon, D.C. Dunand, P. Müllner, *Nat. Mater.* **8**, 863 (2009)
21. K. Bhattacharya, R.D. James, *Science* **307**, 53 (2005)
22. H. Seiner, R. Chulist, W. Maziarz, A. Sozinov, O. Heczko, L. Straka, *Scr. Mater.* **162**, 497 (2019)
23. H. Seiner, *Int. J. Solids Struct.* **221**, 92 (2021)
24. S. Schwabe, R. Niemann, A. Backen, D. Wolf, C. Damm, T. Walter, H. Seiner, O. Heczko, K. Nielsch, S. Fähler, *Adv. Funct. Mater.* **31**, 2005715 (2021)
25. L. Straka, O. Heczko, H. Seiner, N. Lanska, J. Drahokoupil, A. Soroka, S. Fähler, H. Hänninen, A. Sozinov, *Acta Mater.* **59**, 7450 (2011)
26. H. Seiner, L. Straka, O. Heczko, *J. Mech. Phys. Solids* **64**, 198 (2014)
27. O. Heczko, L. Straka, H. Seiner, *Acta Mater.* **61**, 622 (2013)
28. O. Heczko, V. Kopecký, A. Sozinov, L. Straka, *Appl. Phys. Lett.* **103**, 072405 (2013)
29. N. Okamoto, T. Fukuda, T. Kakeshita, *Mater. Sci. Eng. A* **481**, 306 (2008)
30. H. Seiner, M. Zelený, P. Sedlák, L. Straka, O. Heczko, *Phys. Status Solidi Rapid Res. Lett.* **15**, 2100632 (2022)
31. O. Heczko, *Mater. Sci. Technol.* **30**, 1559 (2014)
32. P.J. Brown, J. Crangle, T. Kanomata, M. Matsumoto, K.U. Neumann, B. Ouladdiaf, K.R.A. Ziebeck, *J. Phys. Condens. Matter* **14**, 10159 (2002)
33. L. Righi, F. Albertini, L. Pareti, A. Paoluzi, G. Calestani, *Acta Mater.* **55**, 5237 (2007)
34. P. Veřtát, H. Seiner, L. Straka, M. Klicpera, A. Sozinov, O. Fabelo, O. Heczko, *J. Phys. Condens. Matter* **33**, 265404 (2021)
35. M.A. Uijttewaal, T. Hickel, J. Neugebauer, M.E. Gruner, P. Entel, *Phys. Rev. Lett.* **102**, 035702 (2009)
36. P. Entel, V.D. Buchelnikov, V.V. Khovailo, A.T. Zayak, W.A. Adeagbo, M.E. Gruner, H.C. Herper, E.F. Wassermann, *J. Phys. D* **39**, 865 (2006)
37. A. Saren, A.R. Smith, K. Ullakko, *Microfluid. Nanofluid.* **22**(4), 38 (2018)
38. F. Nilsén, I. Aaltio, S.-P. Hannula, *Compos. Sci. Technol.* **160**, 138 (2018)
39. A. Neudert, Y.W. Lai, R. Schäfer, M. Kustov, L. Schultz, J. McCord, *Adv. Eng. Mater.* **14**, 601 (2012)
40. Y. Ge, O. Heczko, O. Söderberg, S.P. Hannula, *Scr. Mater.* **54**, 2155 (2006)
41. L. Straka, A. Soroka, O. Heczko, H. Hänninen, A. Sozinov, *Scr. Mater.* **87**, 25 (2014)
42. Q. Peng, J. Huang, M. Chen, Q. Sun, *Scr. Mater.* **127**, 49 (2017)
43. C.S. Watson, C. Hollar, K. Anderson, W.B. Knowlton, P. Müllner, *Adv. Funct. Mater.* **23**(32), 3995 (2013)
44. L. Straka, L. Fekete, M. Rameš, E. Belas, O. Heczko, *Acta Mater.* **169**, 109 (2019)
45. S.P. Venkateswaran, N.T. Nuhfer, M. De Graef, *Acta Mater.* **55**, 2621 (2007)
46. H. Seiner, P. Sedlák, L. Bodnárová, J. Drahokoupil, V. Kopecký, J. Kopeček, M. Landa, O. Heczko, *J. Phys. Condens. Matter* **25**, 425402 (2013)
47. L. Bodnárová, P. Sedlák, O. Heczko, H. Seiner, *Shape Mem. Superelast.* **6**, 89 (2020)
48. H.E. Karaca, I. Karaman, B. Basaran, D.C. Lagoudas, Y.I. Chumlyakov, H.J. Maier, *Acta Mater.* **55**, 4253 (2007)
49. P.O. Castillo-Villa, L. Mañosa, A. Planes, D.E. Soto-Parra, J.L. Sánchez-Llamazares, H. Flores-Zúñiga, C. Frontera, *J. Appl. Phys.* **113**, 053506 (2013)
50. W. Sun, J. Liu, B. Lu, Y. Li, A. Yan, *Scr. Mater.* **114**, 1 (2016)
51. R.Y. Umetsu, W. Ito, K. Ito, K. Koyama, A. Fujita, K. Oikawa, T. Kanomata, R. Kainuma, K. Ishida, *Scr. Mater.* **60**, 25 (2009)
52. V. Recarte, J.I. Pérez-Landazábal, V. Sánchez-Alarcos, J.A. Rodríguez-Velamazán, *Acta Mater.* **60**, 1937 (2012)
53. E. Stern-Taulats, P.O. Castillo-Villa, L. Mañosa, C. Frontera, S. Pramanick, S. Majumdar, A. Planes, *J. Appl. Phys.* **115**, 173907 (2014)
54. J. Du, Q. Zheng, W.J. Ren, W.J. Feng, X.G. Liu, Z.D.J. Zhang, *Physica D* **40**, 5523 (2007)
55. J. Liu, T. Gottschall, K.P. Skokov, J.D. Moore, O. Gutfleisch, *Nat. Mater.* **11**(7), 620 (2012)
56. A.S. Turabi, H.E. Karaca, H. Tobe, B. Basaran, Y. Aydogdu, Y.I. Chumlyakov, *Scr. Mater.* **111**, 110 (2016)
57. N.M. Bruno, S. Wang, I. Karaman, Y.I. Chumlyakov, *Sci. Rep.* **7**, 40434 (2017)
58. Z.D. Han, D.H. Wang, C.L. Zhang, S.L. Tang, B.X. Gu, Y.W. Du, *Appl. Phys. Lett.* **89**, 182507 (2006)
59. T. Krenke, E. Duman, M. Acet, X. Moya, L. Mañosa, A. Planes, *J. Appl. Phys.* **102**, 033903 (2007)
60. M. Khan, N. Ali, S. Stadler, *J. Appl. Phys.* **101**, 053919 (2007)
61. D. Bourgault, J. Tillier, P. Courtois, D. Maillard, X. Chaud, *Appl. Phys. Lett.* **96**(13), 132501 (2010)
62. R. Kainuma, K. Oikawa, W. Ito, Y. Sutou, T. Kanomata, K. Ishida, *J. Mater. Chem.* **18**, 1837 (2008)
63. R.Y. Umetsu, X. Xu, R. Kainuma, *Scr. Mater.* **116**, 1 (2016)
64. J. Lyubina, *J. Phys. D* **50**, 053002 (2017)
65. A. Waske, D. Dzekan, K. Sellschopp, D. Berger, A. Stork, K. Nielsch, S. Fähler, *Nat. Energy* **4**, 68 (2019)
66. D. Dzekan, A. Waske, K. Nielsch, S. Fähler, *APL Mater.* **9**, 011105 (2021)
67. M. Gueltig, F. Wendler, H. Ossmer, M. Ohtsuka, H. Miki, T. Takagi, M. Kohl, *Adv. Energy Mater.* **7**, 1601879 (2017)
68. K. Koyama, H. Okada, K. Watanabe, T. Kanomata, R. Kainuma, W. Ito, K. Oikawa, K. Ishida, *Appl. Phys. Lett.* **89**, 182510 (2006)
69. W. Ito, K. Ito, R.Y. Umetsu, R. Kainuma, K. Koyama, K. Watanabe, A. Fujita, K. Oikawa, K. Ishida, T. Kanomata, *Appl. Phys. Lett.* **92**, 021908 (2008)
70. R.Y. Umetsu, K. Ito, W. Ito, K. Koyama, T. Kanomata, K. Ishida, R. Kainuma, *J. Alloys Compd.* **509**, 1389 (2011)
71. M.N. Baibich, J.M. Broto, A. Fert, F.N. Van Dau, F. Petroff, P. Eitenne, G. Creuzet, A. Friederich, J. Chazelas, *Phys. Rev. Lett.* **61**, 2472 (1988)
72. K. Ullakko, *J. Mater. Eng. Perform.* **5**, 405 (1996)
73. S. Breisch, A. Tüysüz, C. Simonidis, *ABB Rev.* **1**, 43 (2022)
74. T. Gottschall, A. Gràcia-Condal, M. Fries, A. Taubel, L. Pfeuffer, L. Manosa, A. Planes, K.P. Skokov, O. Gutfleisch, *Nat. Mater.* **17**(10), 929 (2018)
75. M. Gueltig, H. Ossmer, M. Ohtsuka, H. Miki, K. Tsuchiya, T. Takagi, M. Kohl, *Adv. Energy Mater.* **4**(17), 1400751 (2014)
76. X. Xu, T. Omori, M. Nagasako, T. Kanomata, R. Kainuma, *Appl. Phys. Lett.* **107**, 181904 (2015)
77. T. Odaira, X. Xu, A. Miyake, T. Omori, M. Tokunaga, R. Kainuma, *Scr. Mater.* **153**, 35 (2018)
78. T. Odaira, S. Xu, X. Xu, T. Omori, R. Kainuma, *Appl. Phys. Rev.* **7**, 031406 (2020)
79. I. Takeuchi, O.O. Famodu, J.C. Read, M.A. Aronova, K.-S. Chang, C. Craciunescu, S.E. Lofland, M. Wuttig, F.C. Wellstood, L. Knauss, A. Orozco, *Nat. Mater.* **2**(3), 180 (2003)
80. V. Alexandrakis, J.M. Barandiaran, A. Pérez-Checa, P. Lázpita, P. Decker, S. Salomon, J. Feuchtwanger, A. Ludwig, V. Chernenko, *Scr. Mater.* **178**, 104 (2020)

81. M. Thomas, O. Heczko, J. Buschbeck, L. Schultz, S. Fähler, *Appl. Phys. Lett.* **92**(19), 192515 (2008)
82. S. Schwabe, K. Lünser, D. Schmidt, K. Nielsch, P. Gaal, S. Fähler, What is the speed limit of martensitic transformations? (2022). https://arxiv.org/abs/2202.12581
83. D. Musiienko, A. Saren, L. Straka, M. Vronka, J. Kopeček, O. Heczko, A. Sozinov, K. Ullakko, *Scr. Mater.* **162**, 482 (2019)
84. O. Heczko, L. Straka, O. Soderberg, S.P. Hannula, *SPIE* **5761**, 513 (2005)
85. I. Aaltio, A. Soroka, Y. Ge, O. Söderberg, S.P. Hannula, *Smart Mater. Struct.* **19**, 075014 (2010)
86. K. Ullakko, L. Wendell, A. Smith, P. Müllner, G. Hampikian, *Smart Mater. Struct.* **21**, 115020 (2012)
87. J. Cui, Y.S. Chu, O.O. Famodu, Y. Furuya, J. Hattrick-Simpers, R.D. James, A. Ludwig, S. Thienhaus, M. Wuttig, Z. Zhang, I. Takeuchi, *Nat. Mater.* **5**, 286 (2006)
88. O. Heczko, A. Soroka, S.P. Hannula, *Appl. Phys. Lett.* **93**(2), 022503 (2008)
89. D.C. Dunand, P. Müllner, *Adv. Mater.* **23**(2), 216 (2011)
90. M. Kohl, M. Schmitt, A. Backen, L. Schultz, B. Krevet, S. Fähler, *Appl. Phys. Lett.* **104**, 043111 (2014) □

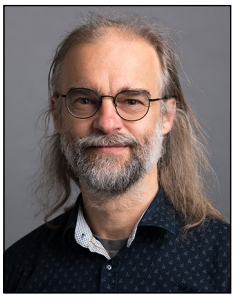

Oleg Heczko is the head of the Department at FZU–Institute of Physics, The Czech Academy of Sciences. He received his PhD degree in 1997 from Charles University, Prague, and spent several years in Finland and Germany. His research mainly focuses on experimental investigation of magnetic materials, including preparation, structure, magnetic, and magnetoelastic properties. Heczko has published more than 200 research articles and holds several patents. He is an acknowledged expert on magnetic shape-memory phenomena, particularly on magnetically induced reorientation, the term he together with Sebastian Fähler coined more than 15 years ago. Heczko can be reached by email at heczko@fzu.cz.

Hanuš Seiner is a research professor and the head of the Department of Ultrasonic Methods at the Institute of Thermomechanics, The Czech Academy of Sciences, Prague. His research covers mainly laser-ultrasonic characterization of smart materials, and theoretical models of martensitic microstructures in these materials. He was awarded the Otto Wichterle Premium for outstanding young scientists by The Czech Academy of Sciences in 2016, and the Fulbright Scholarship in 2017. Seiner can be reached by email at hseiner@it.cas.cz.

Sebastian Fähler studied physics at Georg-August-Universität Göttingen, where he received his PhD degree in 1998. After working at the Leibniz IFW Dresden, he joined the Helmholtz- Zentrum Dresden-Rossendorf in 2021. Fähler is leading a research team on ferroic materials, films, and devices and focuses on thermomagnetic energy harvesting, ferroic cooling, and (magnetic) shape-memory alloys. He coordinated two DFG-funded German Priority Programs, one on magnetic shape-memory alloys (SPP 1239) and one on ferroic cooling (SPP 1599). Fähler can be reached by email at s.faehler@hzdr.de.